Journal of Chromatography A 1673 (2022) 463087

Contents lists available at ScienceDirect

Journal of Chromatography A

journal homepage: www.elsevier.com/locate/chroma

# Separability of stereoisomers by electrokinetic chromatography in presence of a neutral selector – Fundamental aspects assessed by computer simulation

Wolfgang Thormann

*Institute for Infectious Diseases, University of Bern, Bern, Switzerland*

ARTICLE INFO

*Article history:*
Received 9 March 2022
Revised 18 April 2022
Accepted 20 April 2022
Available online 22 April 2022

*Keywords:*
Computer simulation
Chiral separation
Electrokinetic chromatography
Isotachophoresis
Capillary electrophoresis
Cyclodextrin

ABSTRACT

The impact of the two essential parameters, the complexation constant and the mobility of the formed diastereomeric complex, on stereoisomer separation in presence of a neutral chiral selector was assessed by computer simulation for an electrokinetic chromatography configuration with a uniform background electrolyte and one with a cationic discontinues buffer system of isotachophoretic nature. With two enantiomers of norpseudoephedrine as model analytes, data for seven cases featuring complexation in free solution with various combinations of input values, complexation with an immobilized selector and no complexation were analyzed in a hitherto unexplored way. For the uniform buffer study, the determined differences of the effective mobilities and separation selectivities of the stereoisomers were found to be equal to those calculated with the well-known algebraic equations. For the isotachophoretic system with its Kohlrausch adjusted zones, separation is also based on differences in effective mobilities, but the mobility differences cannot be predicted with the same algebraic equation. In both techniques, chiral separations occur due to the presence of the selector and if there is inequality between the mobilities of the transient diastereomeric complexes and the mobility of the free, uncomplexed analyte. Separation of the stereoisomers is possible when complexation constants, complex mobilities or both of these parameters differ. In the isotachophoretic separation a migrating steady-state is formed in which analytes either establish consecutive zones with plateau concentrations or, if present in an insufficient amount, as a peak-like distribution that migrates within a moving steady-state boundary. Simulation data illustrate for the first time the use of a spacer compound that establishes an isotachophoretic zone between enantiomers and thereby provides complete separation of the enantiomers and the possibility of individual detection in peak-mode isotachophoresis. They demonstrate that such an approach could be employed to assess the enantiomeric purity of a chiral compound.



## 1. Introduction

Stereospecific analyte monitoring is widely accomplished via use of chromatographic and electromigration methods and is important in pharmaceutical, pharmacological, forensic, biomedical, agrochemical, environmental and food analysis. For enantiomeric separation under electrokinetic conditions, a chiral selector or a mixture of selectors, proper buffer conditions (pH, ionic strength, micelles, additives etc.) and an ideal temperature are required. In most capillary electrophoresis (CE) approaches, chiral selectors are buffer additives and separations take place in free solution in presence of uniform or discontinuous buffer systems and are collectively referred to as electrokinetic chromatography (EKC). Furthermore, chiral selectors can also be incorporated into a gel matrix, bound to a packing material (referred to as capillary electrochromatography (CEC)) or attached to the inner wall of a capillary (referred to as open tubular CEC) [1–12].

Selectors used in electrokinetic separations include various cyclodextrins (CDs), polysaccharides, proteins, macrocyclic antibiotics, chiral crown ethers, bile acids, chiral surfactants, chiral imprinted polymers and chiral ion-pairing reagents. CDs are the mostly used selectors. They are cyclic oligosaccharides with 6 ($\alpha$-CD), 7 ($\beta$-CD) or 8 ($\gamma$-CD) glucose units that differ in the magnitudes of the cavity and are all chiral, water soluble and UV transparent [13–15]. The three native CDs feature 18, 21 and 24 hydroxy groups, respectively, and have pKa values of 12.33, 12.20

*E-mail address:* wolfgang.thormann@ifik.unibe.ch

https://doi.org/10.1016/j.chroma.2022.463087

and 12.08, respectively [15]. Hydrophilic and hydrophobic regions in these molecules make them extremely versatile as complexing host. Furthermore, CDs can be derivatized randomly or selectively on the hydroxy groups of the CD rims to form neutral CDs with other properties (via alkylation) or charged CDs (via carboxylation, sulfation or other reactions). CDs are able to form intermolecular complexes stereoselectively and these complexes typically exhibit different mobilities compared to the uncomplexed molecules. Thus, native and substituted CDs are widely used as chiral selectors in CE enantioseparations [13–15].

Most interactions between CDs and analytes can be described with a 1:1 (analyte:selector) complexation stoichiometry that are sufficiently fast such that they can be considered instantaneous in comparison to the time scale of electrokinetic movement in electrokinetic capillary setups [7,16–26]. Two one dimensional dynamic simulators for electrophoresis, SIMUL5complex [27,28] and GENTRANS [29], comprise algorithms that include such equilibria in addition to protolysis. These models are based on the principles of electroneutrality and conservation of mass and charge and solve equations that are derived from the transport concepts in solution under the influence of a d.c. electric field together with user-inputted conditions. They can be applied to any initial buffer configuration, including those with buffer discontinuities, and have been used to characterize the migration and separation of enantiomers in EKC [27–30], isotachophoresis (ITP) [29,31–33] and CEC [34], to investigate electromigration dispersion effects caused by complexation [35–38], to study the impact of complex mobilities and complexation constants on migration order [37–39], to elucidate the impact of the complexation of buffer constituents [40,41], to provide insight into the sweeping process of a drug in presence of a neutral CD [42], to study affinity capillary electrophoresis and vacancy affinity capillary electrophoresis methods that are used for the determination of complexation constants [43], to validate the applicability of a new theoretical formula derived from partial-filling affinity capillary electrophoresis for the determination of apparent stability constants of analyte-ligand complexes [44], and to investigate systems with multiply charged CDs [33,45,46,47]. The disadvantage of these simulators is the long execution time interval when configurations mimicking real CE experiments are involved. Alternatively, for the case of systems in which the buffer components are uniformly distributed along the capillary and are present in much higher concentrations than the sample components, a generalized model of the linear theory of electromigration with any equilibria was developed that enables the calculation of positions and shapes of analyte and system peaks in EKC without restrictions on type and number of selectors and their interactions with analyte and buffer components. This model is referred to as PeakMaster 6 [48,49] and enables fast calculations for realistic configurations [30]. These mathematical models require physico-chemical input data for the free and complexed analyte and buffer compounds. Typically, these data have to be determined experimentally or estimated [27–30]. Selected stability constants are also available from the literature (for a compilation of values see [50]).

Enantiomeric separation is based upon differential interaction between analytes and the selector or selectors and/or differences in the migration of the formed diastereomeric complexes. It is worth mentioning that enantioseparation of two stereoisomers in the absence of the binding constant difference with a chiral selector is a unique feature and not seen in chromatographic methods [3,6,8–10,15,26,51,52]. In the present work, the possible impact of the two essential parameters, complexation constant and complex mobility, on stereoisomer separation in presence of a neutral chiral selector was assessed by computer simulation for configurations with (i) a uniform background electrolyte and (ii) a discontinuous buffer system of isotachophoretic nature. The two stereoisomers of the basic drug norpseudoephedrine (NPE) for which input constants for complexation were determined previously in presence of heptakis(2,6-di-O-methyl)-$\beta$-cyclodextrin (DIMEB) [30] were used as model analytes, simulations were performed with PeakMaster 6 (for separations in a uniform buffer only), SIMUL5complex and GENTRANS, and the thereby determined differences of the effective mobilities and separation selectivities of the stereoisomers were compared to those calculated with the well-known algebraic equations. Data for seven cases were generated, namely those (i) without complexation, (ii) with input values determined experimentally, (iii) with an immobilized selector, (iv) with equal complex mobilities, (v) with equal complexation constants, (vi) with equal complex mobilities and complexation constants, and (vii) with both complex mobilities equal to the ionic mobility of NPE.

Discussions about enantiomeric separability in EKC are not new [3,6,7,8,9,10,15–26,51,52]. The simulation data presented in this paper visualize in a hitherto unexplored manner the impact of the complexation constants and complex mobilities on enantiomer separability and the distributions of all zone properties, including the deviation of the neutral selector across the migrating sample zones. They validate the algebraic mobility difference and selectivity equations for the case of uniform buffers, illustrate similarities and differences of chiral separations in EKC and isotachophoretic systems, and represent the first study about the comparability of enantiomer separations in EKC and ITP. Furthermore, configurations with a spacer that establishes an ITP zone between two enantiomers were simulated for the first time and employed to describe peak mode ITP of a minor amount of a stereoisomer, the transition between peak and plateau mode ITP of an enantiomer and the use of this spacer technique to determine the enantiomeric excess of a chiral substance. These new data extend our previous efforts that focused on the separability of the stereoisomers and formation of system peaks in EKC [30] and the isotachophoretic separation process [32].

## 2. Materials and methods

### 2.1. Chemicals and samples

All chemicals used were of analytical or research grade. (1S,2S)-(+)-norpseudoephedrine ((+)-NPE) and (1R,2R)-(-)-norpseudoephedrine ((-)-NPE), both as hydrochloride salts, were from Fluka (Buchs, Switzerland). Heptakis(2,6-di-O-methyl)-$\beta$-cyclodextrin (DIMEB) was from Cyclolab (Budapest, Hungary).

### 2.2. Electrophoretic instrumentation and running conditions

The capillary electrophoresis setup comprised an autosampler PrinCE-C 560 2-Lift (Prince Technologies, Emmen, The Netherland) together with a linear polyacrylamide (LPA) coated fused-silica capillary (Polymicro Technologies, Phoenix, AZ, USA) of 50 $\mu$m I.D. and 83 cm total length, a UVIS 206 PHD absorbance detector (Linear Instruments, Reno, NV, USA) operated at 200 nm and placed at 50.5 cm (60.8% of column length) and a TraceDec conductivity detector (Innovative Sensor Technologies, Strasshof, Austria) at 61.4 cm (74.0% of column length). For EKC with a uniform background electrolyte, the sample was applied at the anodic end via application of pressure (70 mbar for 0.1 min) and runs were executed at ambient temperature (about 25 °C) with application of a constant 20 kV and a concomitant constant coflow with 40 mbar pressure (386.0 µm/s) as described in detail elsewhere [30]. For ITP, the capillary was rinsed with leading electrolyte, the sample was applied at the anodic end via application of pressure (80 mbar for 0.3 min), and the anodic end of the capillary was dipped into the anolyte. A constant current of 2.0 µA was applied as described in [32].

**Table 1**
Physico-chemical input parameters used for simulation.

| Compound | $pK_a$ | Mobility ($10^{-9}$ $m^2$/Vs) | Complexation constant (L/mol) | Complex mobility ($10^{-9}$ $m^2$/Vs) | Ref. |
|---|---|---|---|---|---|
| Sodium | 13.8 | 51.9 | - | - | [b] |
| Acetic acid | 4.76 | 42.4 | - | - | [b] |
| Chloride | -2.00 | 79.1 | - | - | [b] |
| DIMEB | – | 10.0 | - | - | [c] |
| (-)-NPE | 8.90 | 26.5 | 44.7[a] | 4.42[a] | [30,32] |
| (+)-NPE | 8.90 | 26.5 | 66.5[a] | 5.54[a] | [30,32] |

[a] Complex constants and complex mobilities are those for complexation of the protonated bases. Because of the buffer pH used, complexation of the neutral drug species did not have to be considered.
[b] From database of mobilities and pKa values of SIMUL5.
[c] PeakMaster 6 does not require a mobility value for a neutral compound.

### 2.3. Simulation tools and data evaluation

PeakMaster 6 (version 6.0f8, downloaded as freeware from https://echmet.natur.cuni.cz), SIMUL5complex (downloaded as freeware from https://echmet.natur.cuni.cz) and GENTRANS (available from the author upon request) were executed on Windows 10 based 64bit PC's featuring Intel Core i5 or i7 processors. The component's input data for simulations and calculations are summarized in Table 1. For making plots, data were imported into SigmaPlot Scientific Graphing Software version 12.5 (Systat Software, San Jose, CA, USA).

## 3. Results and discussion

### 3.1. Stereoisomer separability in presence of a neutral CD

The separability of the cationic stereoisomers (+)-NPE and (-)-NPE in presence of DIMEB in a uniform buffer and a discontinuous buffer was investigated. The uniform system studied comprised a pH 4.10 background electrolyte composed of 47 mM acetic acid, 8.5 mM NaOH and 16 mM DIMEB as chiral selector. Experimental data with a sample composed of 0.1425 mM of each analyte, 0.285 mM chloride and two-fold diluted background electrolyte without DIMEB are presented in Fig. 1A (for details see Ref. [30]). Alternatively, the NPE stereoisomers could be separated isotachophoretically with the same selector using a leading electrolyte (catholyte) composed of 10 mM NaOH, 24.6 mM acetic acid (pH 4.60) and 10 mM DIMEB together with an anolyte composed of 10 mM acetic acid (pH 3.39) with 10 mM DIMEB (Fig. 1B) [32]. The sample was composed of 2.85 mM of each NPE base and did not contain other components. In both cases, the stereoisomers of NPE were nicely separated and detected via absorbance monitoring (lower graphs) and with the conductivity detector (upper graphs). In absence of DIMED, no separation of (-)-NPE and (+)-NPE was observed (inserts of conductivity data in both panels of Fig. 1).

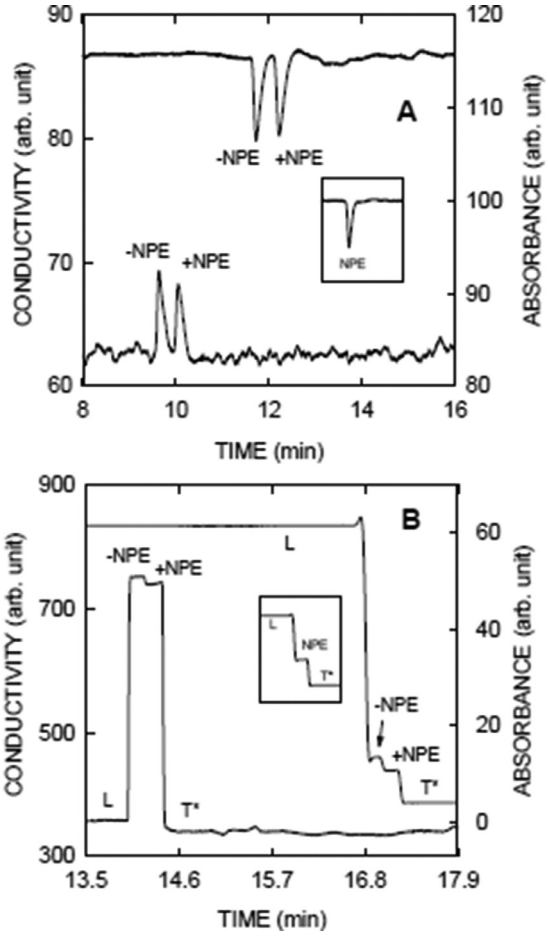


**Fig. 1.** Experimental data for the cationic separation of (+)-NPE and (-)-NPE in (A) a uniform pH 4.10 buffer composed of 47 mM acetic acid, 8.5 mM NaOH and 16 mM DIMEB and (B) an isotachophoretic system with a leader (catholyte) composed of 10 mM NaOH, 24.6 mM acetic acid (pH 4.60) and 10 mM DIMEB, and a terminator (anolyte) with 10 mM acetic acid (pH 3.39) and 10 mM DIMEB. A setup with a 50 µm ID capillary of 83 cm total length with UV (lower graphs) and conductivity (upper graphs) detection at 50.5 cm and 61.4 cm, respectively, was employed. Data of panel A were measured with application of a constant 20 kV and a concomitant constant buffer coflow of 386.0 µm/s (see Ref. [30] for details) whereas those in panel B at a constant current of 2.0 µA (see Ref. [32] for details). The inserts depict conductivity data without DIMEB. -NPE and +NPE represent (-)-NPE and (+)-NPE, respectively. L and T* in panel B refer to leading and adjusted terminating electrolytes, respectively.

With the configuration of Fig. 1A, the effective electrophoretic mobilities of the stereoisomers (-)-NPE and (+)-NPE were determined as function of the selector concentration (0 to 64 mM DIMEB) such that the mobilities of the analyte-DIMEB complexes and the apparent complexation constants could be elucidated [30]. The obtained values are listed in Table 1. The mobility difference of the two stereoisomers as function of the DIMEB concentration can be calculated with the expression [3,6,7,8,16,26]

$$\Delta\mu = \mu_1 - \mu_2 = \left(\left(\mu_f + \mu_{c1}K_1[C]\right)/(1 + K_1[C])\right) - \left(\left(\mu_f + \mu_{c2}K_2[C]\right)/(1 + K_2[C])\right) \quad (1)$$

where $\mu_1$ and $\mu_2$ are the effective mobilities of the stereoisomers 1 and 2, respectively. $K_1$ and $K_2$ are the binding constants between 1 and 2 and the chiral selector, respectively, $\mu_f$ and $\mu_c$ are the mobilities of the free and complexed analyte, respectively, and [C] is the concentration of the chiral selector. This equation reveals the important role of the mobilities in EKC-based enantioseparations. For the NPE stereoisomers, Eq. 1 was plotted with the input data of Table 1 (graph B in Fig. 2A). The largest mobility difference $\Delta\mu = \mu_{\text{-NPE}} - \mu_{\text{+NPE}}$ is 1.607 × $10^{-9}$ $m^2$/Vs and corresponds to a DIMEB concentration of 14.0 mM. The data compare well

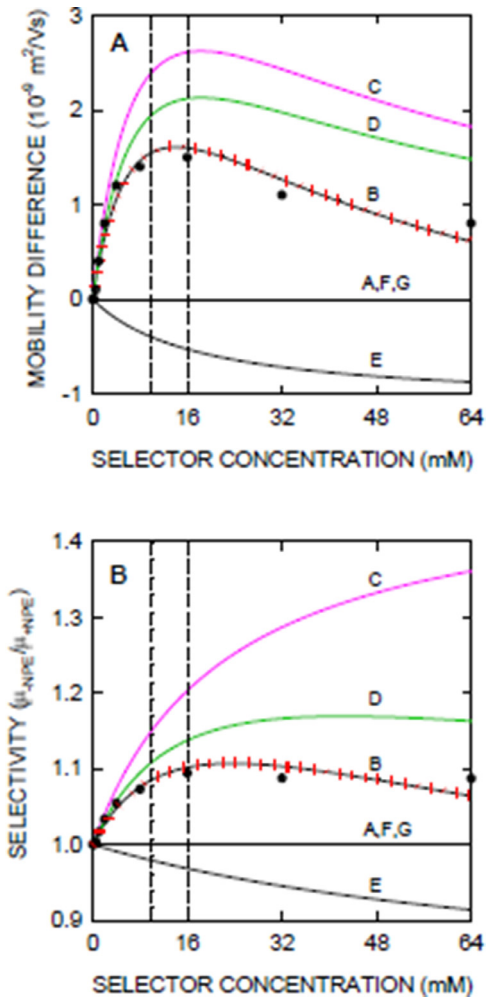


**Fig. 2.** Graphs of (A) effective mobility difference according to Eq. 1 and (B) separation selectivity according to Eq. 2 for the cationic EKC separation of (+)-NPE and (-)-NPE as function of the DIMEB concentration for cases without complexation (graphs A), with the complexation data listed in Table 1 (graphs B), with immobilized DIMEB (graphs C), with equal complex mobilities of 4.98 × $10^{-9}$ m$^2$/Vs (graphs D), with equal complexation constants of 55.60 L/mol (graphs E), with equal complex mobilities of 4.98 × $10^{-9}$ m$^2$/Vs and equal complexation constants of 55.60 L/mol (graphs F), and with both complex mobilities equal to the mobility of NPE (26.5 × $10^{-9}$ m$^2$/Vs; graphs G). The dashed vertical lines at 10 and 16 mM DIMEB represent the chiral selector used in the leader of the isotachophoretic system of Fig. 1B and in the buffer of the EKC system of Fig. 1A, respectively. The black dots represent (A) the mobility difference and (B) the separation selectivity of the experimental data and the red dots those of the nonlinear regression fits presented in Ref. [30]. (For interpretation of the references to colour in this figure legend, the reader is referred to the web version of this article.)

with those obtained via nonlinear regression analysis to the experimental data (fit and experimental values are depicted as red and black dots in Fig. 2A). The graphs for an immobilized selector with $\mu_{c1} = \mu_{c2} = 0$ (graph C of Fig. 2A), with 4.98 × $10^{-9}$ m$^2$/Vs for both complex mobilities (graph D of Fig. 2A), with 55.60 L/mol for both complexation constants (graph E of Fig. 2A), with equal complex mobilities and complexation constants (graph F of Fig. 2A), and with the two complex mobilities equal to the ionic mobility of NPE (26.5 × $10^{-9}$ m$^2$/Vs, graph G of Fig. 2A) are also presented. With no complexation, equal complex mobilities and complexation constants, and the two complex mobilities equal to the ionic mobility of NPE (graphs A, F and G of Fig. 2A, respectively) the mobility difference is zero (no separation of the two stereoisomers) and with equal complexation constants the migration order becomes reversed (graph E in Fig. 2A).

The separation selectivity $\alpha$ is defined as the ratio of the effective mobilities of the two stereoisomers [3,7,9,19,37,39] and, based on Eq. (1), it can be expressed as

$$\alpha = \mu_1/\mu_2 = \big((\mu_f + \mu_{c1}K_1[C])/(1 + K_1[C])\big)/ \big((\mu_f + \mu_{c2}K_2[C])/(1 + K_2[C])\big) \quad (2)$$

Using the values given in Table 1 for NPE provided the graphs in Fig. 2B. The graphs represent the calculated separation selectivity of the NPE stereoisomers for the 0 to 64 mM DIMEB concentration range. According to Eq. 2 (graph B in Fig. 2B), the -NPE stereoisomer is predicted to have a higher effective mobility than +NPE within the entire DIMEB concentration range. These predictions agree well with those observed experimentally (Fig. 1A, red dot graph in Fig. 2B and [30]). Highest separation selectivity is predicted for a DIMEB concentration of 23.5 mM. The graph for an immobilized selector with $\mu c_1 = \mu c_2 = 0$ shows a higher selectivity (graph C of Fig. 2B) and that with 4.98 × $10^{-9}$ m$^2$/Vs for both complex mobilities and otherwise identical conditions as for graph B a selectivity that is between the two (graph D of Fig. 2B). With 55.60 L/mol for both complexation constants results in a selectivity lower than one (graph E of Fig. 2B), a case in which the migration order becomes reversed and is based on the difference of complex mobilities. The selectivity becomes unity for the cases with no complexation, equal complex mobilities and complexation constants, and the two complex mobilities equal to the ionic mobility of NPE (graphs A, F and G of Fig. 2B, respectively).

Both, the data presented in panels A and B of Fig. 2 indicate that a separation of the two NPE stereoisomers is only possible in presence of the chiral selector and if the mobilities of the transient diastereomeric complexes are different than the mobility of free, uncomplexed NPE. With these conditions, separation of the stereoisomers is possible when complexation constants, complex mobilities or both of these parameters differ. The case in which separation is based on the difference in complex mobilities only (graphs E of Fig. 2) is unique and not possible in chromatographic techniques [3,6,8–10,15,26,51,52].

### 3.2. Separability in uniform buffer assessed by simulation

In previous work it was shown that data calculated with PeakMaster 6 for systems with a uniform background electrolyte are in agreement with those of the dynamic simulators SIMUL5complex and GENTRANS [30]. Because the calculations with PeakMaster are executed much faster, PeakMaster 6 was employed to investigate the EKC system of Fig. 1A using a capillary of 83 cm total length, the input data listed in Table 1, a sample composed of 0.285 mM (+)-NPE, 0.1425 mM (-)-NPE, 23.5 mM acetic acid and 4.25 mM NaOH and an applied voltage of 20 kV. The pH 4.10 background electrolyte was composed of 47 mM acetic acid, 8.5 mM NaOH and 16 mM DIMEB. Electropherograms obtained with PeakMaster 6 in absence and presence of 16 mM DIMEB are presented in Fig. 3A and 3B, respectively. No corrections for viscosity differences and the impact of ionic strength on mobility and pKa values were applied for the calculations, and the buffer components (acetic acid and sodium) were assumed not to interact with DIMEB [40,41]. Data presented include the electropherograms based on the concentrations of the NPE stereoisomers and DIMEB (bottom panels in Fig. 3), the concentrations of acetic acid and sodium (center panels of Fig. 3), and conductivity and pH (top panels of Fig. 3). The predicted data are for a detector located at 61.4 cm, for a flow peak detected at 22.625 min (both are for the conductivity detector in the experimental data [30]) and are time-based as obtained in the experiments (Fig. 1A). Without complexation (Fig. 3A), (-)-NPE and (+)-NPE are comigrating and, except for DIMEB, there are small deviations of the background electrolyte properties at the location

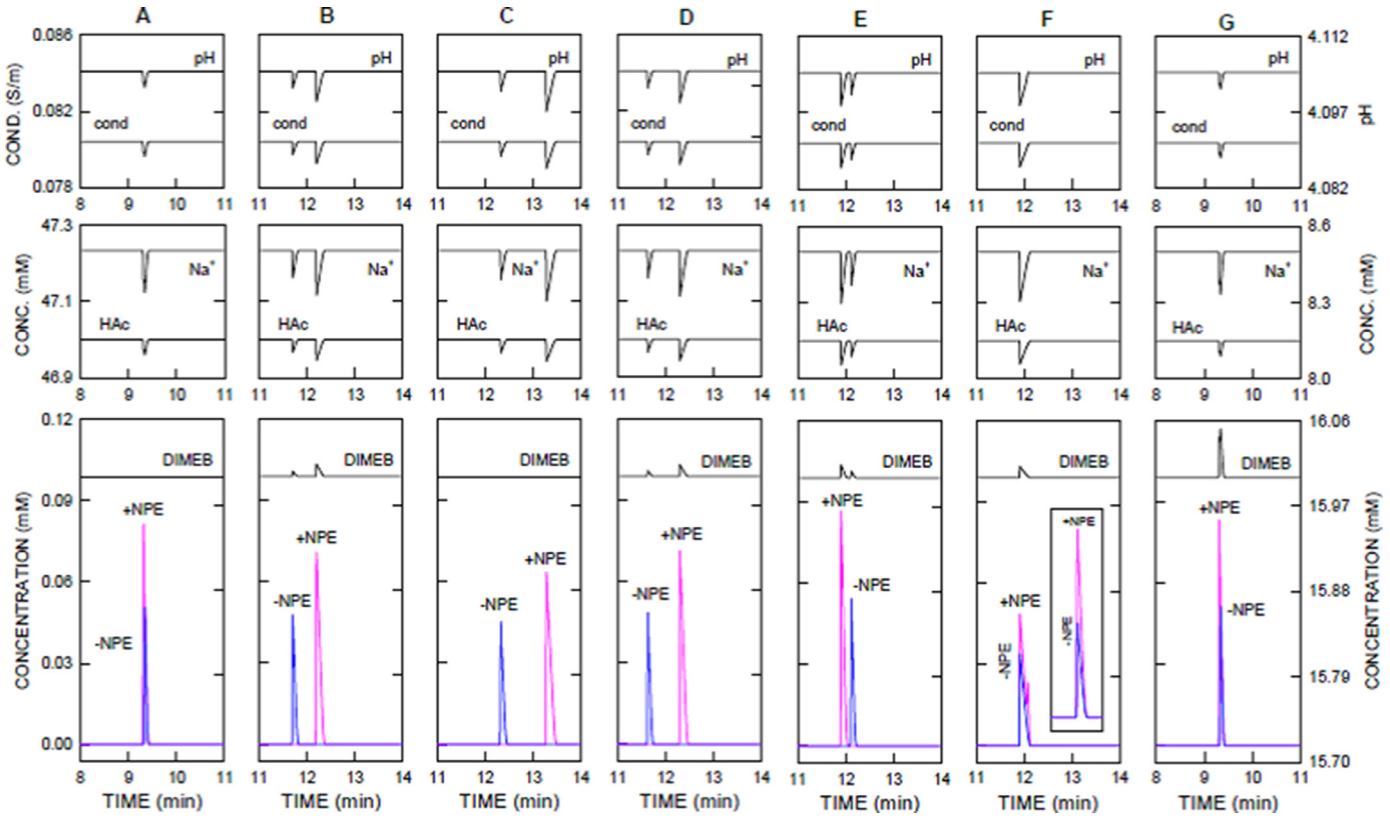


**Fig. 3.** Electropherograms for (+)-NPE and (-)-NPE in a background electrolyte composed of 47 mM acetic acid, 8.5 mM NaOH and 16 mM DIMEB calculated with PeakMaster 6 for a capillary of 83 cm total length and application of 20 kV. (A) without complexation, (B) with the complexation data listed in Table 1, (C) with immobilized DIMEB, (D) with equal complex mobilities (4.98 × $10^{-9}$ $m^2$/Vs), (E) with equal complexation constants (55.60 L/mol), (F) with equal complex mobilities of 4.98 × $10^{-9}$ $m^2$/Vs and equal complexation constants of 55.60 L/mol, and (G) with both complex mobilities equal to the mobility of NPE (26.5 × $10^{-9}$ $m^2$/Vs). Data presented include the profiles of the two stereoisomers ((+)-NPE in pink, (-)-NPE in blue, y-scale on the left side) and DIMEB (y-scale on the right side) in the bottom panels, acetic acid (y-scale on the left side) and NaOH (y-scale on the right side) in the center panels, and conductivity (y-scale on the left side) and pH (y-scale on the right side) in the top panels. The insert in the bottom panel of case F depict comparable detector data for the two stereoisomers simulated by SIMUL5complex. -NPE and +NPE represent (-)-NPE and (+)-NPE, respectively. For explanations refer to text. (For interpretation of the references to colour in this figure legend, the reader is referred to the web version of this article.)

of the migrating stereoisomers. For the conductivity signal, this is in agreement with the experimental observation. With complexation (Fig. 3B), the stereoisomers become separated and retarded compared to the migration without complexation. (-)-NPE with the lower complexation constant is detected ahead of (+)-NPE. This is in agreement with the experimental results. It is important to note that the predicted analyte profiles are not exactly representing the electropherogram monitored by the UV absorbance detector. The absorbance contributions from the buffer changes at the locations of the analytes are not represented by the depicted profiles. Furthermore, zone dispersion under the experimental conditions is larger than in the calculated data because the additional diffusivity caused by the applied flow (Taylor-Aris dispersion [53]) and other dispersing effects are not considered in the calculations of PeakMaster 6. Increased dispersion is observed in the conductivity and the absorbance data presented in Fig. 1A.

Data for analyte mobility calculated with PeakMaster 6, mobility difference and separation selectivity are presented in Table 2. The obtained values of the latter two parameters are the same as those obtained with Eqs. 1 and 2, respectively. It is important to mention that the mobilities provided by PeakMaster 6 are the same as those predicted by SIMUL5complex (data not shown). In addition to the cases A and B of Fig. 3, five other situations were evaluated. CDs can be bound and thus immobilized at the inner wall of a capillary, at the surface of particles used as capillary packing material, or at a monolith present in the capillary. The impact of the 1:1 interaction between NPE and immobilized DIMEB was simulated by setting the complex mobilities to zero or close to zero (0.0001 × $10^{-9}$ $m^2$/Vs) in case of PeakMaster 6. All other input parameters listed in Table 1, including the complexation constants, were assumed to be identical to those in free solution. This provides data that mimic migration and separation with the chiral selector being immobilized to the capillary wall or support material and without unspecific interactions between analytes and the chiral stationary phase. For the studied case, the mobility difference is larger compared to that observed in free solution (compare graphs B and C of Fig. 2A). Data predicted for the NPE system of Fig. 1 with immobilized 16 mM DIMEB are presented in Fig. 3C. For the investigated case, the migration rate is lower and, as predicted by Eq. 1, the mobility difference of the NPE stereoisomers is larger compared with complexation in free solution. The same is true for the separation selectivity $\alpha$ expressed by Eq. 2. Data obtained by PeakMaster 6 are identical to those calculated with the analytical equations (Table 2) and those simulated by SIMUL5complex (data not shown).

The data presented in Fig. 3D were obtained with both complex mobilities having the same value, namely 4.98 × $10^{-9}$ $m^2$/Vs that represents the mean of the two mobilities listed in Table 1 and otherwise identical input data as for Fig. 3B. This illustrates the free solution separation of the two stereoisomers according to the difference of the complexation constants. Resolution is predicted to be larger compared to the case of free solution and smaller than that with the immobilized selector. This is in agreement with the mobility difference calculated by Eq. 1 (compare graph D with graphs B and C of Fig. 2A) and the selectivity ac-

**Table 2**
Effective mobilities for the six investigated EKC cases of Fig. 3.

| Case[a] | EKC example of Fig. 3[b] | | | | $\Delta\mu$[c] | $\alpha$[d] |
|---|---|---|---|---|---|---|
| | $\mu_{-NPE}$ [$10^{-9}$ $m^2$/Vs] | $\mu_{+NPE}$ [$10^{-9}$ $m^2$/Vs] | $\Delta\mu$ ($\mu_{-NPE}$ - $\mu_{+NPE}$) | $\alpha$ ($\mu_{-NPE}$ / $\mu_{+NPE}$) | | |
| A | 26.50 | 26.50 | 0 | 1.00 | 0 | 1.00 |
| B | 17.29 | 15.69 | 1.60 | 1.10 | 1.60 | 1.10 |
| C | 15.45 | 12.84 | 2.61 | 1.20 | 2.61 | 1.20 |
| D | 17.53 | 15.41 | 2.12 | 1.14 | 2.12 | 1.14 |
| E | 16.10 | 16.63 | -0.53 | 0.97 | -0.53 | 0.97 |
| F | 16.37 | 16.37 | 0 | 1.00 | 0 | 1.00 |
| G | 26.50 | 26.50 | 0 | 1.00 | 0 | 1.00 |

[a] Cases according to Figs. 2 and 3.
[b] Data calculated with PeakMaster 6 without nonideality corrections.
[c] Calculated with Eq. (1) for 16 mM DIMEB.
[d] Calculated with Eq. (2) for 16 mM DIMEB.

cording to Eq. 2 (Fig. 2B). The values calculated with both equations are the same as those obtained by PeakMaster 6 (Table 2) and SIMUL5complex (data not shown). In analogy, data with equal complexation constants, 55.60 L/mol (mean of the two values given in Table 1) are depicted in Fig. 3E and represent conditions with the separation being based on the difference in the mobilities of the complexes only. For this case, separation is also possible but the migration order becomes reversed. The mobility difference provides negative values that become larger with increasing selector concentration (graph E in Fig. 2A) and the selectivity is $< 1$ (graph E in Fig. 2B). The calculated values for $\Delta\mu$ and $\alpha$ are listed in Table 2 and are equal to those obtained with the PeakMaster 6 data.

With equal input constants for the two stereoisomers, separation becomes impossible. This is shown with the data of Fig. 3F and graphs F in Fig. 2A and 2B where complexation constants and complex mobilities were assumed to be 55.60 L/mol and $4.98 \times 10^{-9}$ $m^2$/Vs, respectively. The migration rate is smaller compared to the case without complexation depicted in Fig. 3A and is expressed with the lower effective mobilities of the two stereoisomers (Table 2). It was interesting to find that PeakMaster 6 calculated a distorted analyte distribution for (+)-NPE, whereas all other profiles were correct. The correct distribution was obtained with SIMUL5complex (insert in Fig. 3F). Under the given conditions, PeakMaster 6 calculated a fourth system eigenzone with the same effective mobility as NPE. This problem could be avoided by a change of the NaOH buffer concentration to a value $\geq$ 10 mM for which the expected three system peaks and correct analyte distributions were predicted. Finally, with the complex mobilities being equal to the ionic mobility of NPE ($26.5 \times 10^{-9}$ $m^2$/Vs) and otherwise identical conditions as for Fig. 3B, PeakMaster 6 does not calculate a separation of the NPE stereoisomers. Despite the occurring complexation, the effective mobilities of the stereoisomers are identical to uncomplexed NPE (Table 2) and the calculated NPE pattern is equal to that presented in Fig. 3A. As was discussed previously [26], this behavior is also predicted by Eq. 1 and 2 (Table 2).

In addition to the analyte dynamics, simulation provides insight into the distributions of all buffer components, pH and conductivity. The buffer additive responsible for complexation of the analytes, DIMEB, is predicted to deviate from its initial value of 16 mM at the locations of the analytes except for the cases without complexation (Fig. 3A) and immobilized selector (Fig. 3C). The deviation depends on the mobilities of the charged complexes and is highest for the case with the largest mobility (Fig. 3G). This indicates that the migration of the charged complexes produces the DIMEB peaks as was discussed previously [30]. DIMEB itself is neutral and does not migrate under the influence of the electric field. Computer simulation also reveals small deviations of acetic acid and sodium, conductivity and pH across the analyte peaks (Fig. 3).

### 3.3. Separability in isotachophoretic buffer system assessed by simulation

NPE is a weak base that migrates isotachophoretically as cation between sodium as leading constituent, $H_3O^+$ as terminating ion, acetic acid as counter component, and enantioseparation is achieved in presence of DIMEB (Fig. 1B, [32]). The GENTRANS simulation data presented in Fig. 4 were obtained with a leading electrolyte (catholyte) composed of 10 mM NaOH, 24.6 mM acetic acid (pH 4.60) and 10 mM DIMEB. 10 mM acetic acid (pH 3.39) with 10 mM DIMEB served as terminating electrolyte (anolyte). The sample was composed of 2.85 mM of each NPE base and did not contain other components. Simulations were performed with a constant current density of 1000 A/$m^2$ and situations analogous to those of Fig. 3 were assessed. Without complexation, a cationic migrating mixed zone between sodium and the Kohlrausch adjusted acetic acid solution is predicted (Fig. 4A). With the interaction between NPE and DIMEB according to the input data of Table 1, simulation predicts isotachophoretic separation with (-)-NPE (stereoisomer with the lower complexation constant) migrating ahead of (+)-NPE (bottom panel of Fig. 4B). Zone conductivities and pH values of the NPE zones are predicted to be between those of the adjusted terminating zone (28.3 mS/m; 3.14) and the leader (92.0 mS/m, 4.60) (top panel in Fig. 4B). The NPE zones are characterized with sharp front and rear boundaries and the rear boundary features a conductivity dip which is comparable to previously described cationic ITP configurations with $H_3O^+$ as terminating ion [29,31,32]. Simulation data compare well with those observed experimentally (Fig. 1B, [32]). For ITP, the effectivity of separation is focused on mobility difference only (Table 3) because the mobility difference is the fundamental property for separation. Selectivity as defined in Eq. (2) is not used in ITP. A relative selectivity for the transient mixed zone of two analytes was employed to assess optimization in ITP. It represents the relative difference of the effective mobilities in the mixed zone and expresses the maximum relative separation volume [54].

The separation of the NPE stereoisomers simulated in presence of immobilized DIMEB provided the data presented in Fig. 4C. Compared to ITP in free solution, immobilization resulted in zone properties, including NPE concentrations, conductivity and pH, that were somewhat lower (for details refer to Ref. [32]). Furthermore, as the mobility difference is larger as in free solution (Table 3), the boundary between the two stereoisomers is predicted to be sharper (Fig. 4B and 4C). A larger mobility difference was also observed for the corresponding case in EKC (Table 2, Fig. 3C in comparison to Fig. 3B). The data presented in Fig. 4D were obtained with both complex mobilities having the same value ($4.98 \times 10^{-9}$ $m^2$/Vs) together with the complexation constants listed in Table 1 whereas those of Fig. 4E were generated with equal complexation constants (55.60 L/mol) and the complex mo-

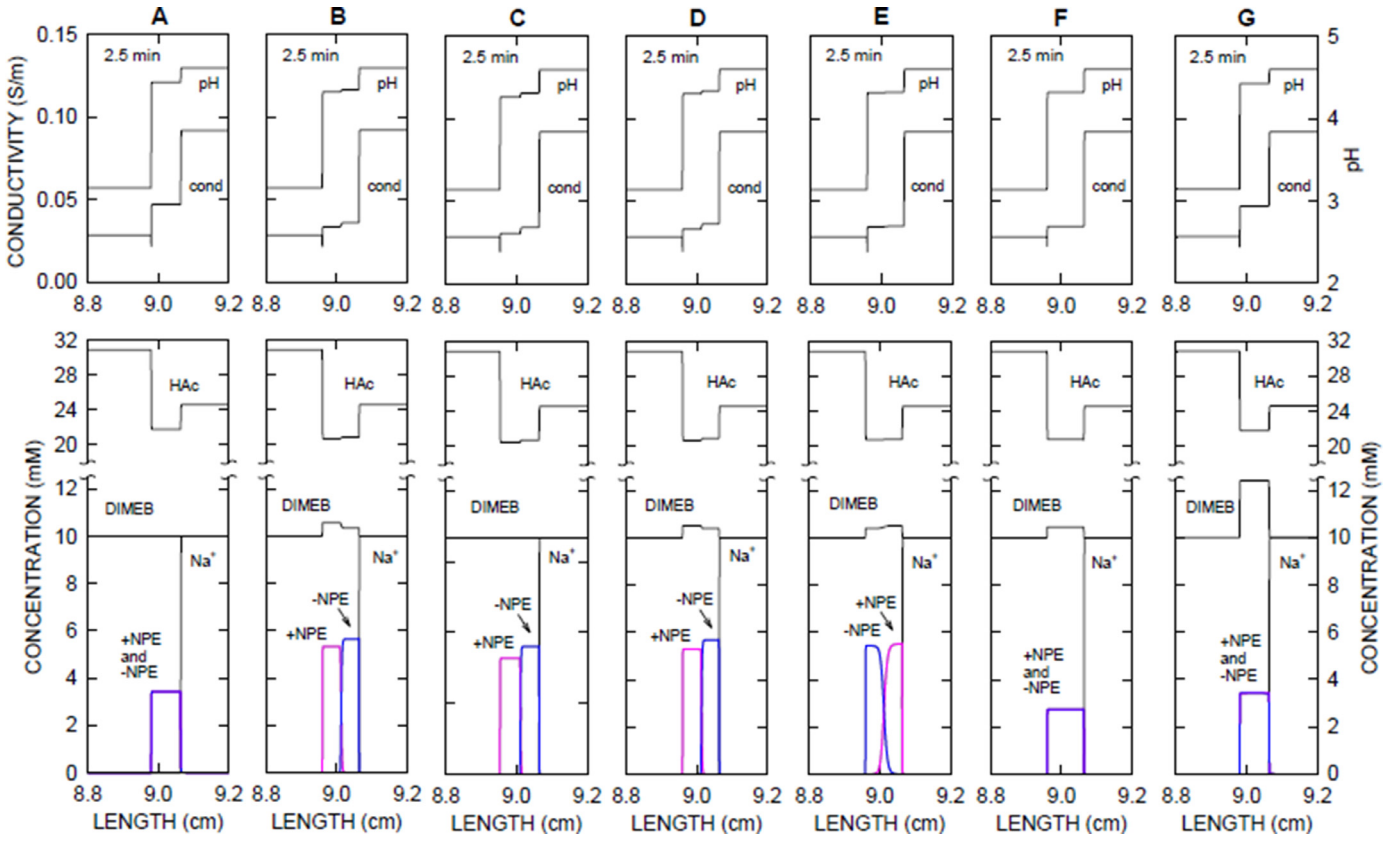


**Fig. 4.** Computer predicted isotachophoretic separation of the NPE stereoisomers utilizing a pH 4.60 leading electrolyte (catholyte) composed of 10.0 mM NaOH, 24.6 mM acetic acid and 10 mM DIMEB. A mixture of 10.0 mM acetic acid and 10 mM DIMEB served as terminating electrolyte (anolyte) and the sample comprised (+)-NPE and (-)-NPE as bases (2.85 mM each). The simulations were performed at a constant current density of 1000 A/m$^2$, without EOF and for 2.5 min of current flow in a column of 10 cm length that was divided into 20,000 segments. Data were obtained (A) without complexation, (B) with the complexation data listed in Table 1, (C) with immobilized DIMEB, (D) with equal complex mobilities (4.98 × 10$^{-9}$ m$^2$/Vs), (E) with equal complexation constants (55.60 L/mol), (F) with equal complex mobilities of 4.98 × 10$^{-9}$ m$^2$/Vs and equal complexation constants of 55.60 L/mol, and (G) with both complex mobilities equal to the mobility of NPE (26.5 × 10$^{-9}$ m$^2$/Vs). Data presented include the profiles of the two stereoisomers ((+)-NPE in pink, (-)-NPE in blue), $Na^+$, DIMEB and acidic acid in the bottom panels. Conductivity (y-scale on the left side) and pH (y-scale on the right side) profiles are depicted in the top panels. -NPE and +NPE represent (-)-NPE and (+)-NPE, respectively. (For interpretation of the references to colour in this figure legend, the reader is referred to the web version of this article.)

**Table 3**
Effective mobilities for the six investigated isotachophoretic cases of Fig. 4[a].

| Case[b] | Steady-state zones[c] | | | $\Delta\mu$[d] | Transient mixed zones[c] | | |
|---|---|---|---|---|---|---|---|
| | $\mu_{-NPE}$ [10$^{-9}$ m$^2$/Vs] | $\mu_{+NPE}$ [10$^{-9}$ m$^2$/Vs] | $\Delta\mu$ ($\mu_{-NPE}$ - $\mu_{+NPE}$) | | $\mu_{-NPE}$ [10$^{-9}$ m$^2$/Vs] | $\mu_{+NPE}$ [10$^{-9}$ m$^2$/Vs] | $\Delta\mu$ ($\mu_{-NPE}$ - $\mu_{+NPE}$) |
| A | 26.50 | 26.50 | 0 | 0 | - | - | - |
| B | 20.29 | 18.86 | 1.43 | 1.55 | 20.32 | 18.82 | 1.50 |
| C | 19.20 | 17.11 | 2.09 | 2.40 | 19.28 | 17.02 | 2.26 |
| D | 20.43 | 18.68 | 1.75 | 1.95 | 20.48 | 18.62 | 1.86 |
| E | 19.32 | 19.66 | -0.34 | -0.40 | 19.32 | 19.68 | -0.36 |
| F | 19.50 | 19.50 | 0 | 0 | - | - | - |
| G | 26.50 | 26.50 | 0 | 0 | - | - | - |

[a] For all mobility entries, the units are 10$^{-9}$ m$^2$/Vs
[b] Cases according to Fig. 4
[c] Data determined with SIMUL5complex for a system with sodium as leading component (mobility of 51.90 × 10$^{-9}$ m$^2$/Vs) and $H_3O^+$ as terminating component with an effective mobility of 16.70 × 10$^{-9}$ m$^2$/Vs (calculated with Eq. 8 of Ref. [58]).
[d] Calculated with Eq. 1 for 10 mM DIMEB.

bilities of Table 1. The latter data revealed a migration order inversion as was the case for the EKC system of Fig. 3E. Furthermore, the mobility difference of the two NPE stereoisomers is much smaller (Table 3) which results in a much broader boundary between the two NPE zones. Simulation with equal complexation constants (55.60 L/mol) and equal complex mobilities (4.98 × 10$^{-9}$ m$^2$/Vs) predicted a migrating steady-state mixed zone and no separation of the stereoisomers (Fig. 4F). The predicted mobility is 19.50 × 10$^{-9}$ m$^2$/Vs and thus lower compared to that of the free NPE ion (Table 3). The plateau concentration of both NPE stereoisomers is lower (2.74 mM, Fig. 4F) compared to that in absence of complexation (3.42 mM, Fig. 4A). Finally, with both complex mobilities equal to that of the free NPE ion (26.50 × 10$^{-9}$ m$^2$/Vs), there is no separation of the two NPE stereoisomers despite the occurring differential complexation with DIMEB (Fig. 4G). They migrate as in absence of complexation with a mobility of 26.50 × 10$^{-9}$ m$^2$/Vs.

The formed (-)-NPE and (+)-NPE sample zones not only differ in the plateau concentration, pH, conductivity, and acetic acid concentration, but also in the concentration of DIMEB (Fig. 4). DIMEB

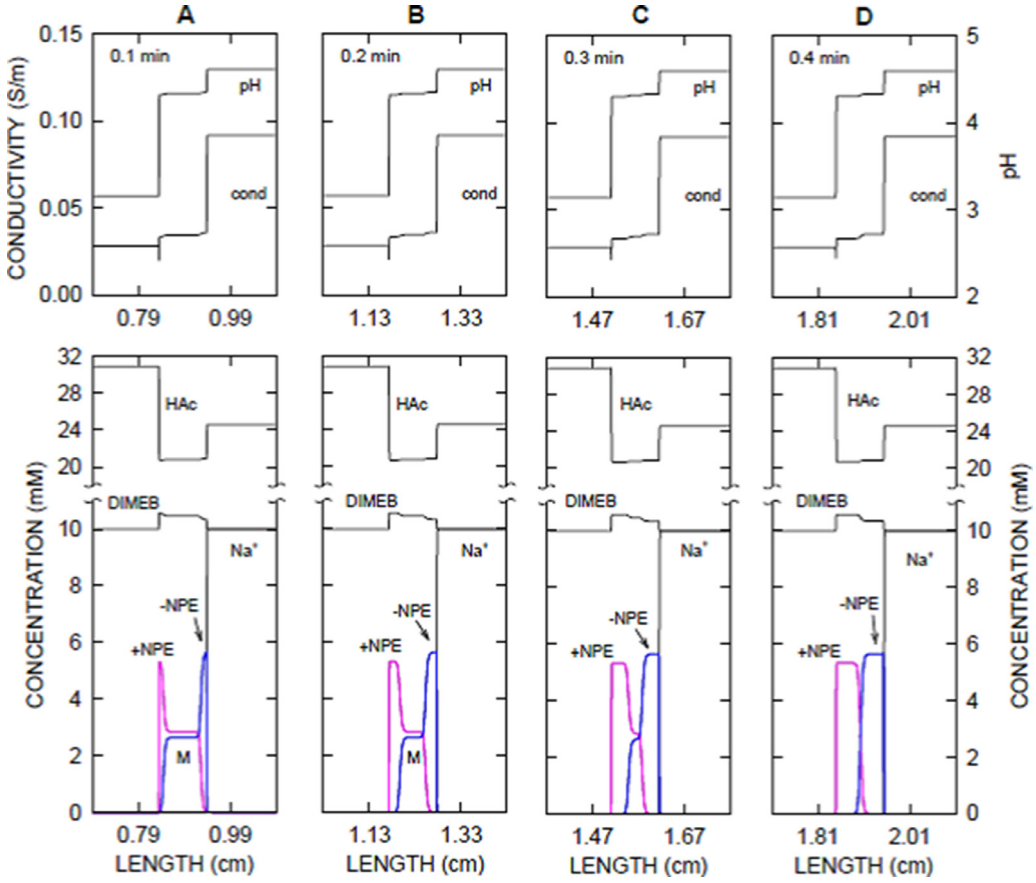


**Fig. 5.** Isotachophoretic separation process of the NPE stereoisomers for the system of Fig. 4B (input data of Table 1) at (A) 0.1 min, (B) 0.2 min, (C) 0.3 min, and (D) 0.4 min of application of a constant current density of 1000 A/m$^2$. M refers to the transient mixed zone. Key as for Fig. 4.

is neutral and does not migrate under the influence of the electric field. The DIMEB increase inside the ITP zones compared to its 10 mM value in the leading and terminating zones is due to the migration of the charged complexes [31,32]. Highest deviation in DIMEB was predicted for the case in which the complex mobilities were assumed to be equal to the ionic mobility of NPE (Fig. 4G). This is in analogy to the EKC data presented in Fig. 3. The data further reveal, that the DIMEB deviation is both a function of the complex mobility (Fig. 4E) and the complexation constant (Fig. 4D).

Separation of two compounds in ITP is based upon differential migration and proceeds via a migrating transient mixed zone which is formed according to the regulating principle [54–57]. This principle also holds for enantiomeric separations [31,32]. For the example of Fig. 4B, this is illustrated with the simulation data presented in Fig. 5. The properties of the mixed zone, including its conductivity, are distinctly different to the properties of the pure zones of (-)-NPE and (+)-NPE which are gradually formed in front of and behind the mixed zone, respectively. The mixed zone becomes smaller with time and vanishes when the separation of the two stereoisomers is completed as was discussed in detail previously [32]. This is illustrated with the data presented in panels A to D of Fig. 5. After 0.4 min of current flow (Fig. 5D), the separation is almost completed. The boundary between the two stereoisomers, however, is not yet at steady-state. Its shape is still significantly broader compared to that shown in Fig. 4B. Once steady-state is reached, the separated stereoisomers continue to migrate as a steady-state migrating zone pattern between sodium with an effective mobility of 51.9 $\times$ 10$^{-9}$ m$^2$/Vs and $H_3O^+$ as terminating component with the effective mobility of 16.70 $\times$ 10$^{-9}$ m$^2$/Vs (calculated with Eq. (8) of Ref. [58]). Table 3 lists effective mobility values of the two NPE stereoisomers at steady-state and during separation. For cases B to D of Fig. 4, the effective mobility of (-)-NPE is larger than that of (+)-NPE at steady-state and during separation. The opposite is true for case E of Fig. 4. All mobility values are larger than that of $H_3O^+$ as well as smaller compared to the mobility of sodium such that the two stereoisomers separate and migrate isotachophoretically. Values calculated with Eq. (1) for the mobility difference in presence of 10 mM DIMEB are also listed in Table 3 and are shown to be higher compared to those established with the moving boundary-based regulation principle. Thus, Eq. (1) cannot be used to predict the mobility difference for the isotachophoretic separation.

In an isotachophoretic system, separated stereoisomers migrate as adjacent zones as is illustrated with the data presented in Figs. 4 and 5. Enantiomer zones can also be separated with a spacer compound that has an effective mobility between those of the stereoisomers. This is depicted here for the first time with the computer simulation data presented in Fig. 6. The example presented in Fig. 6A corresponds to the case of Fig. 4B. The spacer used represents a weak base with a p$K_a$ value of 8.9 and a mobility of 19.4 $\times$ 10$^{-9}$ m$^2$/Vs, was added at a concentration of 3 mM to the sample, and was assumed not to interact with DIMEB. The spacer is depicted to form an isotachophoretic zone between those of (-)-NPE and (+)-NPE (Fig. 6A). The use of a spacer is important for separation of enantiomers that are not applied in sufficient amounts such that they form a zone with a plateau concentration (for general information about the use of spacers in ITP see [59,60]). This is illustrated with the data presented in Fig. 6B and 6C. They were obtained with a 10-fold lower sample load (0.285 mM of each NPE stereoisomer instead of the 2.85 mM em-

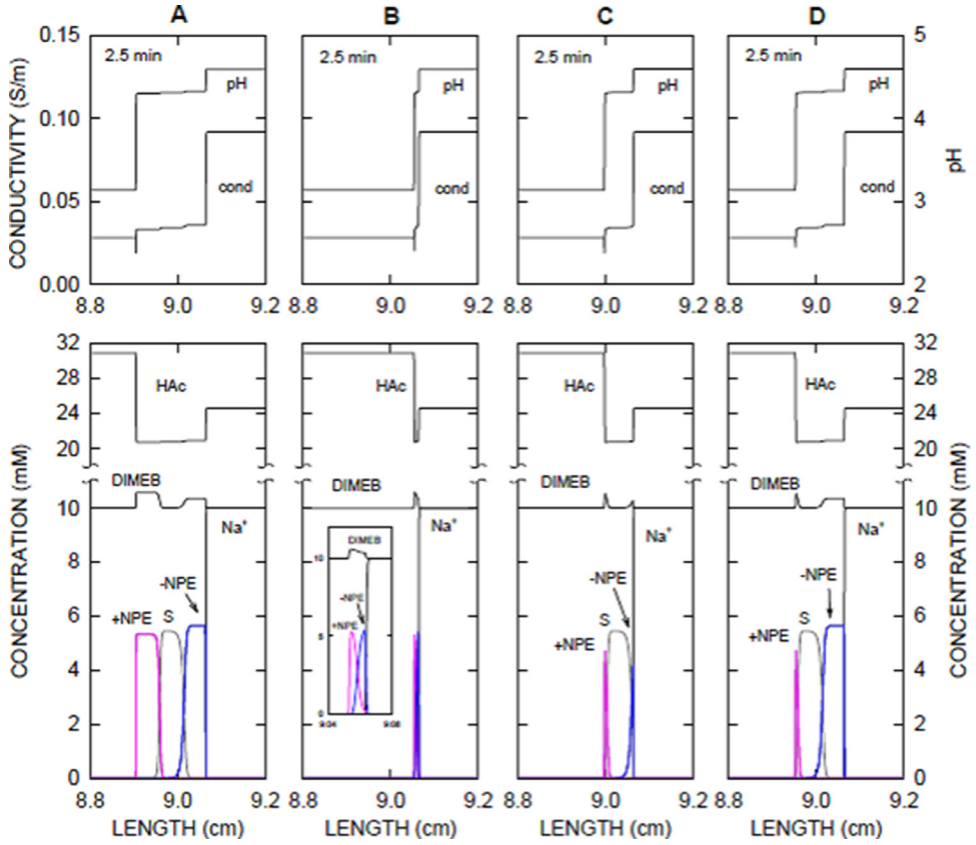


**Fig. 6.** Isotachophoretic separation of the NPE stereoisomers (input data of Table 1, and for 2.5 min of current flow at a constant current density of 1000 A/m$^2$) having as sample (A) 2.85 mM of both NPE stereoisomers and 3 mM spacer, (B) 0.285 mM of both stereoisomers, (C) 0.285 mM of both stereoisomers and 3 mM spacer, (D) 2.85 mM (-)-NPE, 0.285 mM (+)-NPE and 3 mM spacer. Other conditions as for Fig. 4B. S refers to the spacer (dark grey line) with a mobility of 19.4 × $10^{-9}$ m$^2$/Vs. For explanations refer to text. (For interpretation of the references to colour in this figure legend, the reader is referred to the web version of this article.)

ployed for the patterns in Fig. 4B and 6A). Without spacer, (-)-NPE and (+)-NPE do not completely separate (Fig. 6B) and cannot be detected individually. With the spacer, complete separation is obtained (Fig. 6C, both stereoisomers migrate in the isotachophoretic peak mode) and the two stereoisomers could be monitored via absorbance or fluorescence detection if the optical properties of the spacer and buffer components do not interfere with those of the analytes or possibly also by MS according to the principle demonstrated recently for non-chiral cationic isotachophoretic separations [60].

The spacer is also essential for analysis of stereoisomer mixtures in which one stereoisomer is present in a quantity to be able to form a zone with plateau concentration whereas the second stereoisomer in the sample features a lower concentration and migrates in the peak mode. This is illustrated with the data presented in Fig. 6D. (-)-NPE and (+)-NPE were sampled at concentrations of 2.85 and 0.285 mM, respectively. With the aid of the spacer, the two NPE stereoisomers can be completely separated. Due to the Kohlrausch adjustment, the analytes become concentrated, (-)-NPE to the plateau concentration of 5.33 mM (Fig. 6A and 7A, 1.87-fold enrichment compared to the initial sample concentration) and the minor stereoisomer (+)-NPE to a peak level of 4.73 mM (16.6-fold concentration) (Figs. 6D and 7B). With (+)-NPE sample concentrations of 28.5 µM, 2.85 µM and 0.285 µM and otherwise identical conditions as for Fig. 6D, simulation predicts a concentration to 1.012, 0.113 and 0.011 mM, respectively (Fig. 7C, 7D and 7E, respectively, with about 36-fold concentration enhancement). The 1000 A/m$^2$ employed for the simulations corresponds to a current of 2 µA applied to a 50 µm ID capillary (conditions of Fig. 1B) and represents a realistic value. The thickness of an ITP boundary is

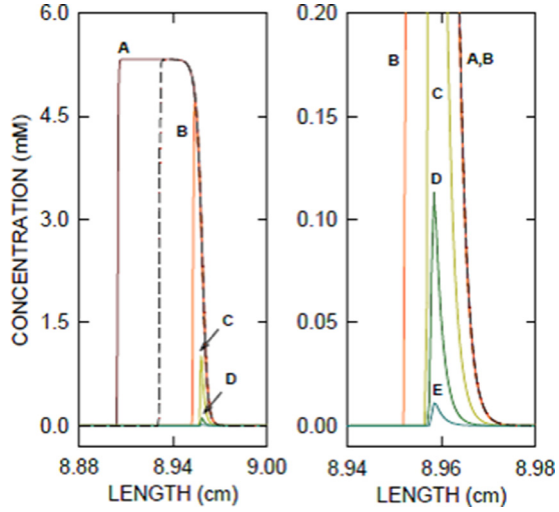


**Fig. 7.** Isotachophoretic steady-state concentration distributions of (+)-NPE for samples composed of 2.85 mM (-)-NPE, 3 mM spacer and (A) 2.85 mM (+)-NPE, (B) 0.285 mM (+)-NPE, (C) 28.5 µM (+)-NPE, (D) 2.85 µM (+)-NPE, and (E) 0.285 µM (+)-NPE. Simulation conditions were otherwise the same as those used for Fig. 4B and Fig. 6.

inversely proportional to the current density applied [61]. Application of a higher current density would sharpen the boundaries and result in higher peaks of compounds that migrate in the peak mode. The application of a larger sample zone would also result in higher sensitivity. This might, however, require a longer separa-

tion distance which is the location of the first boundary when the separation is completed and represents the first column position at which the state-state zone pattern can be detected [55,56].

The ITP spacer technique could be used to determine the enantiomeric excess (ee) which is a measurement of the purity of chiral substances. It reflects the degree to which a sample contains one enantiomer in greater amounts than the other. In practice, it is most often expressed as a percent enantiomeric excess (%ee). For the examples of Fig. 6D and 7, %ee can be calculated as $((c_{-NPE} - c_{+NPE})/(c_{-NPE} + c_{+NPE}))*100$ [7]. The racemic mixture has an %ee of 0%, while the examples with 0.285 mM, 28.5 µM, 2.85 µM and 0.285 µM +NPE have %ee values of 81.82%, 98.02%, 99.80% and 99.98%, respectively. Thus, the sample with the smallest (+)-NPE concentration corresponds to an almost pure (-)-NPE stereoisomer. In peak mode ITP, the area under the peak represents a measure for analyte quantitation (Fig. 7). In the plateau mode, the zone length is proportional to the sampled amount. This is shown with the broken line graph in Fig. 7 that was obtained with a (+)-NPE sample concentration of 1.425 mM.

The determination of the stereoisomeric purity of compounds is one of the predominant applications of EKC enantioseparations. EKC-based assays are reported to be suitable for the detection of the order of 0.1% of an enantiomeric impurity (for reviews see [9,13,62]). This sensitivity is reached easily in ITP as is demonstrated for the case shown in Fig. 7D in which the peak concentration is predicted to be 0.113 mM. EKC simulation data for the studied NPE example of Fig. 1A with a sample comprising 2.85 µM of the minor enantiomer reveal that its peak concentration is not higher than 3 µM (data not shown). Thus, in order to reach the same peak concentration as in ITP, requires a stacking procedure that provides a large concentration enhancement. Further work is required to explore the potential of ITP for that purpose. This includes the search for real substances that act as spacers and the demonstration of a possible superiority to EKC.

## 4. Conclusions

The impact of the two essential parameters, the complexation constant and the complex mobility, on stereoisomer separation in presence of a neutral chiral selector was assessed by computer simulation for a configuration with a uniform background electrolyte and one with a cationic discontinues buffer system of isotachophoretic nature. For two stereoisomers of NPE as model analytes, data for seven cases were analyzed, namely those (i) without complexation, (ii) with input values determined experimentally, (iii) with an immobilized selector, (iv) with equal complex mobilities, (v) with equal complexation constants, (vi) with equal complex mobilities and complexation constants, and (vii) with the two complex mobilities equal to the ionic mobility of NPE. PeakMaster 6 and SIMUL5complex were employed for the uniform buffer study and the thereby determined differences of the effective mobilities and separation selectivities of the stereoisomers were found to be equal to those calculated with the wellknown algebraic equations. GENTRANS and SIMUL5complex served as the simulators for the isotachophoretic system in which separation is also based on differences in effective mobilities. Separation criteria are the same in both systems. This is illustrated here with the analogy of the simulation data presented in Fig. 3 and Fig. 4. Chiral separations occur due to the presence of the selector and if the mobilities of the transient diastereomeric complexes are different than the mobility of free, uncomplexed NPE. Separation of the stereoisomers is possible when complexation constants, complex mobilities or both of these parameters differ.

Chiral EKC separations progress while the stereoisomers migrate through the buffer and they become resolved completely if the mobility difference is large enough. In an isotachophoretic separation a migrating steady-state is formed in which analytes either establish consecutive zones with plateau concentrations or, if present in an insufficient amount, as a peak-like distribution that migrates within a moving steady-state boundary. In the latter case, a spacer that establishes an ITP zone between the enantiomers is required for complete separation and individual detection. Data presented for the NPE system illustrate that behavior and demonstrate that such an approach could be employed to assess the enantiomeric purity of a chiral compound. This principle was shown here for the first time.

Simulation continuous to be an invaluable tool to provide insight into electrophoretic processes. A requirement for computer prediction of chiral separations is the availability of realistic input data, particularly complexation constants and mobilities of the free and complexed molecules. If such data are not available from the literature, they have to be determined experimentally or estimated. All data presented in this paper were assessed with a uniform distribution of the selector. The effects of analyte complexation and migration along a gradient of the neutral selector is not discussed here, but has been dealt with previously for CEC [34] and isotachophoretic [32] systems.

The simulators used in this work are based on 1:1 (analyte:selector) interactions between analytes and CDs that are sufficiently fast such that they can be considered instantaneous in comparison to the time scale of electrokinetic movement. Other complexation stoichiometries and very slow analyte CD complexation reactions are also possible [63,64]. The simulators would have to be modified to simulate such systems.

## Credit author statement

**Wolfgang Thormann**: Conceptualization, simulations, manuscript writing.

## Declaration of Competing Interest

The authors declare that they have no known competing financial interests or personal relationships that could have appeared to influence the work reported in this paper.

## Funding

This research did not receive any specific grant from funding agencies in the public, commercial, or not-for-profit sectors.

## References

[1] J. Snopek, I. Jelínek, E. Smolková-Keulemansová, Chiral separation by analytical electromigration methods, J. Chromatogr. 609 (1992) 1–17, doi:10.1016/0021-9673(92)80145-K.
[2] S. Fanali, Identification of chiral drug isomers by capillary electrophoresis, J. Chromatogr. A 735 (1996) 77–121, doi:10.1016/0021-9673(95)01327-x.
[3] B. Chankvetadze, Separation selectivity in chiral capillary electrophoresis with charged selectors, J. Chromatogr. A 792 (1997) 269–295, doi:10.1016/S0021-9673(97)00752-8.
[4] V. Schurig, S. Mayer, Separation of enantiomers by open capillary electrochromatography on polysiloxane-bonded permethyl-beta-cyclodextrin, J. Biochem. Biophys. Methods 48 (2001) 117–141, doi:10.1016/s0165-022x(01)00144-0.
[5] A. Rizzi, Fundamental aspects of chiral separations by capillary electrophoresis, Electrophoresis 22 (2001) 3079–3106, doi:10.1002/1522-2683(200109)22:15(3079::AID-ELPS3079)3.0.CO;2-F.
[6] B. Chankvetadze, G. Blaschke, Enantioseparations in capillary electromigration techniques: recent developments and future trends, J. Chromatogr. A 906 (2001) 309–363, doi:10.1016/S0021-9673(00)01124-9.
[7] G.K.E. Scriba, Selected fundamental aspects of chiral electromigration techniques and their application to pharmaceutical and biomedical analysis, J. Pharm. Biomed. Anal. 27 (2002) 373–399, doi:10.1016/S0731-7085(01)00653-7.
[8] B. Chankvetadze, Enantioseparations by using capillary electrophoretic techniques. The story of 20 and a few more years, J. Chromatogr. A 1168 (2007) 45–70, doi:10.1016/j.chroma.2007.08.008.

[9] G.K.E. Scriba, Fundamental aspects of chiral electromigration techniques and application in pharmaceutical and biomedical analysis, J. Pharm. Biomed. Anal. 55 (2011) 688–701, doi:10.1016/j.jpba.2010.11.018.

[10] S. Fanali, B. Chankvetadze, Some thoughts about enantioseparations in capillary electrophoresis, Electrophoresis 40 (2019) 2420–2437, doi:10.1002/elps.201900144.

[11] S. Bernardo-Bermejo, E. Sánchez-López, M. Castro-Puyana, M.L. Marina, Chiral capillary electrophoresis, Trends Anal. Chem. 124 (2020) 115807, doi:10.1016/j.trac.2020.115807.

[12] N. de Koster, C.P. Clark, I. Kohler, Past, present, and future developments in enantioselective analysis using capillary electromigration techniques, Electrophoresis 42 (2021) 38–57, doi:10.1002/elps.202000151.

[13] G.K.E. Scriba, Cyclodextrins in capillary electrophoresis enantioseparations – Recent developments and applications, J. Sep. Sci. 31 (2008) 1991–2011, doi:10.1002/jssc.200800095.

[14] S. Fanali, Chiral separations by CE employing CDs, Electrophoresis 30 (2009) S203–S210, doi:10.1002/elps.200900056.

[15] P. Peluso, B. Chankvetadze, Native and substituted cyclodextrins as chiral selectors for capillary electrophoresis enantioseparations: structures, features, application, and molecular modeling, Electrophoresis 42 (2021) 1676–1708, doi:10.1002/elps.202100053.

[16] S.A.C. Wren, R.C. Rowe, Theoretical aspects of chiral separation in capillary electrophoresis. 1. Initial evaluation of a model, J. Chromatogr. 603 (1992) 235–241, doi:10.1016/0021-9673(92)85366-2.

[17] S.A.C. Wren, R.C. Rowe, R.S. Payne, A theoretical approach to chiral capillary electrophoresis with some practical implications, Electrophoresis 15 (1994) 774–778, doi:10.1002/elps.11501501108.

[18] Y.Y. Rawjee, D.U. Staerk, G. Vigh, Capillary electrophoretic chiral separations with cyclodextrin additives. 1. Acids - chiral selectivity as a function of pH and the concentration of beta-cyclodextrin for fenoprofen and ibuprofen, J. Chromatogr. 635 (1993) 291–306, doi:10.1016/0021-9673(93)80372-F.

[19] Y.Y. Rawjee, R.L. Williams, G. Vigh, Capillary electrophoretic chiral separations using beta-cyclodextrin as resolving agent. 2. Bases - chiral selectivity as a function of pH and the concentration of beta-cyclodextrin, J. Chromatogr. A 652 (1993) 233–245, doi:10.1016/0021-9673(93)80664-T.

[20] B.A. Williams, G. Vigh, Dry look at the CHARM (charged resolving agent migration) model of enantiomer separations by capillary electrophoresis, J. Chromatogr. A 777 (1997) 295–309, doi:10.1016/S0021-9673(97)00424-X.

[21] F. Lelièvre, P. Gareil, A. Jardy, Selectivity in capillary electrophoresis: Application to chiral separations with cyclodextrins, Anal. Chem. 69 (1997) 385–392, doi:10.1021/ac960606z.

[22] P. Dubský, J. Svobodová, B. Gaš, Model of CE enantioseparation systems with a mixture of chiral selectors. Part I. Theory of migration and interconversion, J. Chromatogr. B 875 (2008) 30–34, doi:10.1016/j.jchromb.2008.07.018.

[23] P. Dubský, J. Svobodová, E. Tesařová, B. Gaš, Enhanced selectivity in CZE multichiral selector enantioseparation systems: proposed separation mechanism, Electrophoresis 31 (2010) 1435–1441, doi:10.1002/elps.200900742.

[24] P. Dubský, L. Müllerová, M. Dvorák, B. Gaš, Generalized model of electromigration with 1:1 (analyte:selector) complexation stoichiometry: Part I. Theory, J. Chromatogr. A 1384 (2015) 142–146, doi:10.1016/j.chroma.2015.01.029.

[25] L. Müllerová, P. Dubský, B. Gaš, Generalized model of electromigration with 1:1 (analyte:selector) complexation stoichiometry: Part II. Application to dual systems and experimental verification, J. Chromatogr. A 1384 (2015) 147–154, doi:10.1016/j.chroma.2015.01.055.

[26] B. Chankvetadze, Contemporary theory of enantioseparations in capillary electrophoresis, J. Chromatogr. A 1567 (2018) 2–25, doi:10.1016/j.chroma.2018.07.041.

[27] V. Hruška, M. Beneš, J. Svobodová, I. Zusková, B. Gaš, Simulation of the effects of complex-formation equilibria in electrophoresis: I. Mathematical model, Electrophoresis 33 (2012) 938–947, doi:10.1002/elps.201100529.

[28] J. Svobodová, M. Beneš, V. Hruška, K. Ušelová, B. Gaš, Simulation of the effects of complex-formation equilibria in electrophoresis: II. Experimental verification, Electrophoresis 33 (2012) 948–957, doi:10.1002/elps.201100503.

[29] M.C. Breadmore, H.Y. Kwan, J. Caslavska, W. Thormann, Dynamic high-resolution computer simulation of electrophoretic enantiomer separations with neutral cyclodextrins as chiral selectors, Electrophoresis 33 (2012) 958–969, doi:10.1002/elps.201100472.

[30] J. Caslavska, W. Thormann, Contemporary chiral simulators for capillary zone electrophoresis, Electrophoresis 41 (2020) 502–513, doi:10.1002/elps.201900363.

[31] J. Caslavska, M.C. Breadmore, W. Thormann, Dynamic high-resolution computer simulation of isotachophoretic enantiomer separation and zone stability, Electrophoresis 35 (2014) 625–637, doi:10.1002/elps.201300438.

[32] J. Caslavska, R.A. Mosher, W. Thormann, Computer simulation of the isotachophoretic migration and separation of norpseudoephedrine stereoisomers with a free or immobilized neutral chiral selector, J. Chromatogr. A 1623 (2020) 461176, doi:10.1016/j.chroma.2020.461176.

[33] S. Mikkonen, J. Caslavska, P. Gebauer, W. Thormann, Inverse cationic ITP for separation of methadone enantiomers with sulfated $\beta$-cyclodextrin as chiral selector, Electrophoresis 40 (2019) 659–667, doi:10.1002/elps.201800387.

[34] W. Thormann, J. Caslavska, R.A. Mosher, Computer simulation of electrophoretic aspects of enantiomer migration and separation in capillary electrochromatography with a neutral selector, Electrophoresis 36 (2015) 773–783, doi:10.1002/elps.201400457.

[35] V. Hruška, J. Svobodová, M. Beneš, B. Gaš, A nonlinear electrophoretic model for PeakMaster: Part III. Electromigration dispersion in systems that contain a neutral complex-forming agent and a fully charged analyte, Theory, J. Chromatogr. A 1267 (2012) 102–108, doi:10.1016/j.chroma.2012.06.086.

[36] M. Beneš, J. Svobodová, V. Hruška, M. Dvořák, I. Zusková, B. Gaš, A nonlinear electrophoretic model for PeakMaster: Part IV. Electromigration dispersion in systems that contain a neutral complex-forming agent and a fully charged analyte. Experimental verification, J. Chromatogr. A 1267 (2012) 109–115, doi:10.1016/j.chroma.2012.06.053.

[37] J. Svobodová, M. Beneš, P. Dubský, G. Vigh, B. Gaš, Simulation of the effects of complex-formation equilibria in electrophoresis: III. Simultaneous effects of chiral selector concentration and background electrolyte pH, Electrophoresis 33 (2012) 3012–3020, doi:10.1002/elps.201200293.

[38] M. Riesová, J. Svobodová, K. Ušelová, Z. Tošner, I. Zusková, B. Gaš, Determination of thermodynamic values of acidic dissociation constants and complexation constants of profens and their utilization for optimization of separation conditions by simul 5 complex, J. Chromatogr. A. 1364 (2014) 276–288, doi:10.1016/j.chroma.2014.08.070.

[39] W. Thormann, L. Chankvetadze, M. Gumustas, B. Chankvetadze, Dynamic computer simulation of electrophoretic enantiomer migration order and separation in presence of a neutral cyclodextrin, Electrophoresis 35 (2014) 2833–2841, doi:10.1002/elps.201400193.

[40] M. Beneš, R. Riesová, J. Svobodová, E. Tesařová, P. Dubský, B. Gaš, Complexation of buffer constituents with neutral complexation agents: Part II. Practical impact in capillary zone electrophoresis, Anal. Chem. 85 (2013) 8526–8534, doi:10.1021/ac401381d.

[41] M. Riesová, J. Svobodová, Z. Tošner, M. Beneš, E. Tesařová, B. Gaš, Complexation of buffer constituents with neutral complexation agents: Part I. Impact on common buffer properties, Anal. Chem. 85 (2013) 8518–8525, doi:10.1021/ac4013804.

[42] M. Boublík, M. Riesová, P. Dubský, B. Gaš, Enhancement of the conductivity detection signal in capillary electrophoresis systems using neutral cyclodextrins as sweeping agents, Electrophoresis 39 (2018) 1390–1398, doi:10.1002/elps.201800027.

[43] M. Dvorák, J. Svobodová, M. Beneš, B. Gaš, Applicability and limitations of affinity capillary electrophoresis and vacancy affinity capillary electrophoresis methods for determination of complexation constants, Electrophoresis 34 (2013) 761–767, doi:10.1002/elps.201200581.

[44] M. Ansorge, P. Dubský, K. Ušelová, Into the theory of the partial-filling affinity capillary electrophoresis and the determination of apparent stability constants of analyte-ligand complexes, Electrophoresis 39 (2018) 742–751, doi:10.1002/elps.201700385.

[45] J. Šesták, R. Theurillat, F.A. Sandbaumhüter, W. Thormann, Fundamental aspects of field-amplified electrokinetic injection of cations for enantioselective capillary electrophoresis with sulfated cyclodextrins as selectors, J. Chromatogr. A 1558 (2018) 85–95, doi:10.1016/j.chroma.2018.05.022.

[46] S. Mikkonen, J. Caslavska, V. Hruška, W. Thormann, Computer simulation and enantioselective capillary electrophoresis to characterize isomer mixtures of sulfated $\beta$-cyclodextrins, Electrophoresis 39 (2018) 770–778, doi:10.1002/elps.201700376.

[47] S. Mikkonen, W. Thormann, Computer simulation of the enantioselective separation of weak bases in an online capillary electrophoresis based microanalysis configuration comprising sulfated cyclodextrin as selector, Electrophoresis 39 (2018) 1482–1487, doi:10.1002/elps.201800113.

[48] M. Malý, M. Dovhunová, M. Dvořák, G.S. Gerlero, P.A. Kler, V. Hruška, P. Dubský, Generalized model of the linear theory of electromigration and its application to electrokinetic chromatography: Theory and software PeakMaster 6 - Next Generation, Electrophoresis 40 (2019) 683–692, doi:10.1002/elps.201800400.

[49] M. Dovhunová, M. Malý, P. Dubský, G.S. Gerlero, P.A. Kler, Generalized model of the linear theory of electromigration and its application to electrokinetic chromatography: Capillary zone electrophoretic systems with complex forming equilibria, J. Chromatogr. A 1610 (2020) 460595, doi:10.1016/j.chroma.2019.460595.

[50] K. Ušelová-Včeláková, I. Zusková, B. Gaš, Stability constants of amino acids, peptides, proteins, and other biomolecules determined by CE and related methods: Recapitulation of published data, Electrophoresis 28 (2007) 2145–2152, doi:10.1002/elps.200600780.

[51] B. Chankvetadze, W. Lindner, G.K.E. Scriba, Enantiomer separations in capillary electrophoresis in the case of equal binding constants of the enantiomers with a chiral selector: Commentary on the feasibility of the concept, Anal. Chem. 76 (2004) 4256–4260, doi:10.1021/ac0355202.

[52] K. Lomsadze, A.B. Martínez-Girón, M. Castro-Puyana, L. Chankvetadze, A.L. Crego, A. Salgado, M.L. Marina, B. Chankvetadze, About the role of enantioselective selector–selectand interactions and the mobilities of diastereomeric associates in enantiomer separations using CE, Electrophoresis 30 (2009) 2803–2811, doi:10.1002/elps.200900076.

[53] J. Caslavska, R.A. Mosher, W. Thormann, Impact of Taylor-Aris diffusivity on analyte and system zone dispersion in CZE assessed by computer simulation and experimental validation, Electrophoresis 36 (2015) 1529–1538, doi:10.1002/elps.201500034.

[54] P. Gebauer, P. Boček, Optimization in isotachophoresis. The concept of selectivity and separation speed, J. Chromatogr. 320 (1985) 49–65, doi:10.1016/S0021-9673(01)90479-0.

[55] W. Thormann, D. Arn, E. Schumacher, Monitoring of the isotachophoretic separation of two components with an array detector, Sep. Sci. Technol. 19 (1984) 995–1011, doi:10.1080/01496398408058343.
[56] W. Thormann, Principles of isotachophoresis and of the isotachophoretic separation of two components, Sep. Sci. Technol. 19 (1984) 455–467, doi:10.1080/01496398408060328.
[57] T. Hirokawa, K. Nakahara, Y. Kiso, The separation process in isotachophoresis 2. Binary-mixtures and transient state models, J. Chromatogr. 463 (1989) 51–71, doi:10.1016/S0021-9673(01)84453-8.
[58] P. Boček, P. Gebauer, M. Deml, Concept of the effective mobility of the hydrogen ion and its use in cationic isotachophoresis, J. Chromatogr. 219 (1981) 21–28, doi:10.1016/S0021-9673(00)80569-5.
[59] R.A. Mosher, D.A. Saville, W. Thormann, The Dynamics of Electrophoresis, VCH Publishers, Weinheim, 1992.
[60] Z. Malá, P. Gebauer, Capillary isotachophoresis with electrospray-ionization mass-spectrometric detection: cationic electrolyte systems in the medium-alkaline range for selective analysis of medium strong bases, J. Chromatogr. A 1618 (2020) 460907, doi:10.1016/j.chroma.2020.460907.
[61] W. Thormann, R.A. Mosher, Theoretical and computer aided analysis of steady state moving boundaries in electrophoresis: an analytical solution for the estimation of boundary widths between weak electrolytes, Trans. Soc. Computer Simulation 1 (1984) 83–96.
[62] L. Blomberg, H. Wan, Determination of enantiomeric excess by capillary electrophoresis, Electrophoresis 21 (2000) 1940–1952, doi:10.1002/1522-2683(20000601)21:10⟨1940::AID-ELPS1940⟩3.0.CO;2-#.
[63] S. Krait, A. Salgado, C. Villani, L. Naumann, C. Neusüß, B. Chankvetadze, G.K.E. Scriba, Unusual complexation behavior between daclatasvir and $\gamma$ -Cyclodextrin. A multiplatform study, J. Chromatogr. A. 1628 (2020) 461448, doi:10.1016/j.chroma.2020.461448.
[64] S. Krait, A. Salgado, P. Peluso, M. Malanga, T. Sohajda, G. Benkovics, L. Naumann, C. Neusüß, B. Chankvetadze, G.K.E. Scriba, Complexation of daclatasvir by single isomer methylated $\beta$-cyclodextrins studied by capillary electrophoresis, NMR spectroscopy and mass spectrometry, Carbohydr. Polym. 273 (2021) 118486, doi:10.1016/j.carbpol.2021.118486.